Liquid Interface for Accurate Intrinsic Thermal Conductivity Measurements of Polymer Films Using the Transient Plane Source Method

ASME Journal of Thermal Science and Engineering Applications
Online journal at:
https://asmedigitalcollection.asme.org/thermalscienceapplication

Liquid Interface for Accurate Intrinsic Thermal Conductivity Measurements of Polymer Films Using the Transient Plane Source Method

Zijin Zeng[1]
Department of Chemistry and Chemical Engineering,
Chalmers University of Technology,
Gothenburg 41296, Sweden;
Hot Disk AB,
SvenHultins Gatan 9A,
Gothenburg 41288, Sweden
e-mail: zijin@chalmers.se

Przemyslaw Sowinski
Department of Chemistry and Chemical Engineering,
Chalmers University of Technology,
Gothenburg 41296, Sweden
e-mail: sowinski@chalmers.se

Christian Müller
Department of Chemistry and Chemical Engineering,
Chalmers University of Technology,
Gothenburg 41296, Sweden
e-mail: christian.muller@chalmers.se

Besira Mihiretie[1]
Hot Disk AB,
SvenHultins Gatan 9A,
Gothenburg 41288, Sweden
e-mail: besira.mihiretie@hotdiskinstruments.com

Characterizing the thermal properties of micrometer-thin films is crucial for optimizing their performance in a broad range of engineering applications. The transient plane source (TPS) method is widely used for measuring bulk materials, but its direct application to thin films fails due to thermal contact resistance. By comparing TPS measurements across films of varying thicknesses, it is possible to compensate for the influence of thermal contact resistance and extract the intrinsic thermal conductivity. However, this method still suffers from significant errors, e.g., as high as 26% in case of polyolefin films, since its underlying assumption—thermal contact resistance remains identical for films of different thickness—does not always hold true for actual measurements. Here, we demonstrate that these errors can be effectively reduced to 4% by incorporating a liquid thermal interface material. Specifically, the intrinsic cross-plane thermal conductivities of high-density polyethylene, isotactic polypropylene, and regioregular poly(3-hexylthiophene) films are determined to be 0.450, 0.277, and 0.296 W/(m · K), respectively. Moreover, these measurements exhibit remarkable reproducibility, achieving a standard deviation below 0.02 W/(m · K) when the film thickness is sufficiently varied. Furthermore, potential systematic errors are investigated through a comprehensive numerical study. Overall, this study offers critical insights that considerably extend the applicability of TPS measurements for thin films. [DOI: 10.1115/1.4069207]

Keywords: heat conduction, transient plane source method, measurement techniques, heat and mass transfer, thermophysical properties

1 Introduction

Polymer films with micrometer-scale thickness play an important role in various engineering applications, with their mechanical, electrical, optical, and thermal properties significantly impacting their performance [1]. Among these properties, the thermal conductivity is of particular importance, especially in the fields of energy harvesting/storage and electronics [2–4]. For instance, in the case of fuel cells, the thermal conductivities of proton exchange membranes and gas diffusion layers critically influence the internal temperature distribution and thus the device performance [5,6]. Similarly, in the case of organic thermoelectric generators, the thermal conductivity governs the temperature difference across the generator, impacting the efficiency of power generation [7,8]. Furthermore, recent studies have demonstrated that insulating polymer films processed in the solid state can feature a high thermal conductivity, thereby facilitating the thermal management of electronics [9–11].

There are numerous measurement techniques available for assessing the thermal conductivity of micrometer-thick films [12–20]. They can be broadly categorized into contact and contactless methods, depending on whether the sensing element physically contacts the specimen or not [12,20]. Contactless methods, predominantly based on optics, include time-domain thermoreflectance [13,14], frequency-domain thermoreflectance [15–17], and laser flash analysis (LFA) [18,19,21]. One of the common advantages of contactless methods is the disregard of thermal contact resistance (R_C) between the specimen and the sensing element [12,20]. Yet, these methods often require the deposition of a transducer layer (e.g., gold [22,23], aluminum [24,25], graphite [26]) on the sample surface. This layer facilitates the conversion of thermal responses into detectable optical signals, which however tends to increase both the time and complexity of the measurement process.

Contact methods include the guarded hot plate (GHP) method [27], the 3ω method [28,29], the temperature wave analysis (TWA) method [30], and the transient plane source (TPS) method [31]. The GHP method is a steady-state method with the advantages

[1]Corresponding authors.

Manuscript received April 16, 2025; final manuscript received July 17, 2025; published online August 4, 2025. Assoc. Editor: Stephen A Solovitz.

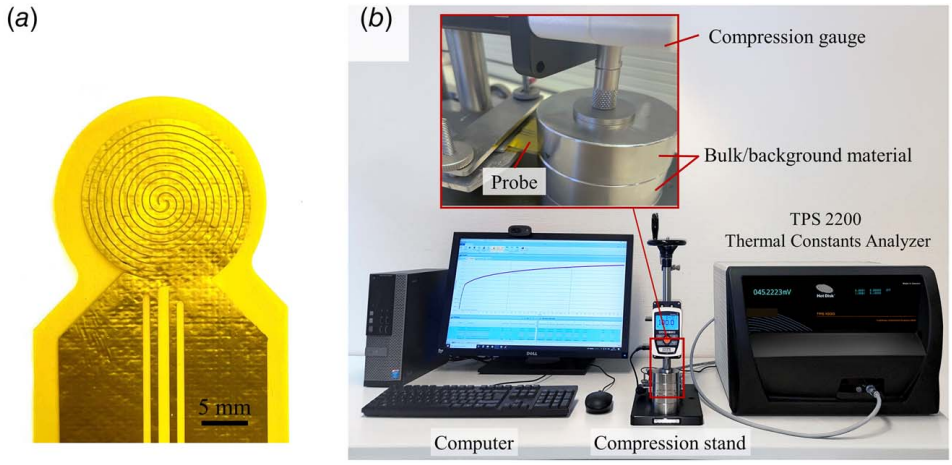

Fig. 1 (*a*) Probe profile featuring a nickel bifilar spiral sandwiched between polyimide layers and (*b*) the configuration of a TPS measurement using a compression stand

of simplicity and high accuracy [27]. The 3ω method, a frequency-dependent technique, necessitates a metal sensor deposited on the sample surface. This method allows for the measurement of the thermal conductivity of submicrometer-thick films, which are thinner than those measurable by other contact methods [28,29]. TWA is another frequency-dependent method for film specimens that is only employed for cross-plane thermal diffusivity measurements. The determination of thermal conductivity is achieved by multiplying the measured thermal diffusivity with the volumetric heat capacity [32].

The TPS method in turn is a time-dependent technique offering versatile and nondestructive testing [31,33,34]. Initially developed for characterizing bulk materials, it has been extended to determine the cross-plane thermal conductivity of films with a thermal conductivity ranging from 0.05 W/(m · K) to 2 W/(m · K) [31,35–37].

TPS measurements utilize a probe made of a nickel spiral covered by insulation layers that provide electrical insulation and mechanical support (Fig. 1(*a*)). When measuring bulk materials, this probe is positioned between two identical specimens and a mounting force is applied to enhance physical contact within the specimen–probe assembly (Fig. 1(*b*)). The probe heats the specimens through the Joule heating, and the resulting thermal response of the probe ($\Delta T(t)$) is simultaneously recorded over time [31] (Fig. 2(*a*)). ΔT can be further written as a function of dimensionless time τ (Fig. 2(*b*)), which is normalized with respect to the probe radius (r) and thermal diffusivity (α) of the bulk material [31,37]

$$\Delta T(\tau) = \Delta T_a + P(\pi^{3/2} r\lambda)^{-1} D(\tau)$$
$$\text{where} \quad \tau = (t/\theta)^{1/2}, \quad \theta = r^2/\alpha \tag{1}$$

where P represents the power output of the probe, λ is the thermal conductivity of the bulk material, and ΔT_a is the additional temperature increase caused by the total thermal resistance between the probe and the bulk material. ΔT_a reaches a constant value shortly after the measurement begins [31]. $D(\tau)$ is a function of dimensionless time τ, which depends on the type of probe [31,33]

$$D(\tau) = \int_0^\tau d\sigma\sigma^{-2} \int_0^1 v dv \int_0^1 u du \times \exp\left(-\frac{u^2+v^2}{4\sigma^2}\right) I_0\left(\frac{uv}{2\sigma^2}\right) \tag{2}$$

where σ is an integration variable related to dimensionless time. The variables v and u are normalized radial coordinates, and I_0 is a modified Bessel function.

To determine the thermal properties of the bulk material, a least-squares iterative process is employed to fit the recorded $\Delta T(t)$ using Eq. (1). This fitting process establishes a linear relationship between $\Delta T(\tau)$ and $D(\tau)$. The slope of the linear relationship is associated with the thermal conductivity of the bulk material, while its intercept at $D(\tau) = 0$ reveals the additional temperature increase ΔT_a (Fig. 2(*b*)). ΔT_a can be utilized to estimate the total thermal resistance (R_{tot}) between the probe and the bulk material, which impedes heat conduction from the probe to the bulk material [31,37]

$$P = 2S\Delta T_a / R_{tot} \tag{3}$$

where S is the area of the probe.

Equation (3) assumes that heat conduction between the probe and the bulk material is one-dimensional (1D). This assumption holds when the thickness of the insulation layer is markedly smaller than the probe diameter. However, this simplification can introduce errors that vary with the thickness and thermal conductivity of the sample [38].

To determine the thermal conductivity of thin films, a two-step process is employed. First, the background material is measured, which is referred to as the background measurement (Fig. 2(*c*)). By performing the fitting process on the thermal response data ($\Delta T_b(t)$, Fig. 2(*a*)), the additional temperature increase ($\Delta T_{a,b}$, Fig. 2(*b*)) is obtained. This increase is further used to estimate the total thermal resistance ($R_{tot,b}$), which consists of the thermal resistance caused by the insulation layer (R_i) and the thermal contact resistance between the probe and bulk material (R_{c-b})

$$R_{tot,b} = R_i + R_{c,p\text{-}b} \tag{4}$$

Then, two thin-film specimens, e.g., two polymer films, are positioned between the probe and the background material while keeping the measurement conditions unchanged (Fig. 2(*d*), referred to as the film measurement). Similarly, the thermal response data ($\Delta T_f(t)$, Fig. 2(*a*)) are obtained to estimate the additional temperature increase ($\Delta T_{a,\ f}$, Fig. 2(*b*)) and the total thermal resistance ($R_{tot,f}$). $R_{tot,f}$ in this case can then be written as

$$R_{tot,f} = R_i + R_{c,p\text{-}f} + R_f + R_{c,f\text{-}b} \tag{5}$$

where $R_{c,p\text{-}f}$ is the thermal contact resistance between the probe and the film specimen, $R_{c,f\text{-}b}$ denotes the thermal contact resistance between the film and the background material, and R_f represents the thermal resistance caused by the film specimen. The intrinsic cross-plane thermal conductivity ($\lambda_\perp$) of the films is given by

$$R_f = \delta/\lambda_\perp \tag{6}$$

where δ is the thickness of the film specimen. However, introducing the film specimens imposes an additional thermal contact resistance (denoted as C) compared to the background measurement.

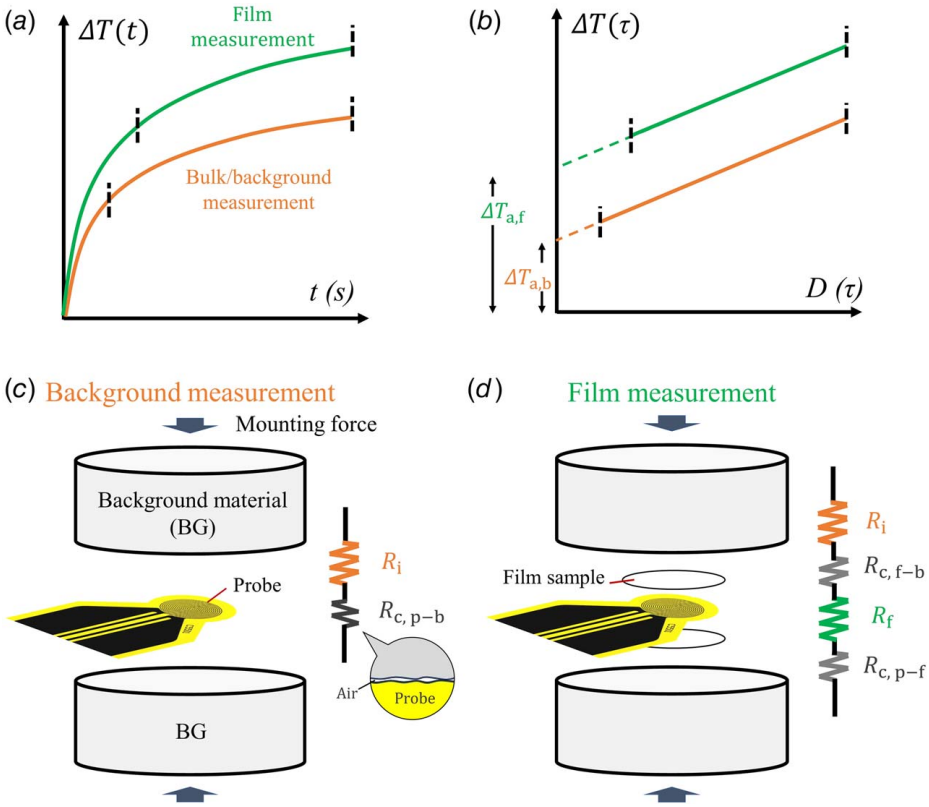

Fig. 2 (*a*) Thermal response of the probe over time (*t*) during a background measurement and a film measurement, respectively. The thick dashed lines define the range of data utilized for determining the properties of the bulk/background material; (*b*) thermal response of the probe as a function of dimensionless time (τ) in a background measurement and a film measurement, respectively. The intercepts ($\Delta T_{a,f}$, $\Delta T_{a,b}$) are utilized for determining the properties of the film specimens; (c) schematic of a background measurement and its thermal network between the probe and the background material. The inset illustrates the contact between the BG and the probe; (*d*) schematic of a film measurement and the corresponding thermal network.

Mathematically, this can be expressed as

$$R_{\text{tot,f}} - R_{\text{tot,b}} = \delta/\lambda_{\perp} + C = \delta/\lambda_{\perp,\text{a}} \tag{7}$$

In the current approach, the TPS method directly measures the apparent thermal conductivity ($\lambda_{\perp,\text{a}}$) of the film. This value includes the effect of the additional thermal contact resistance and as a result the measured thermal conductivity is typically lower than the intrinsic cross-plane thermal conductivity [38,39].

Determining the intrinsic cross-plane thermal conductivity using the TPS method is feasible by comparing measurements of films with varying thickness [39,40]. This approach, referred to as the slope method, has been reported to achieve an accuracy of approximately 7–15% [39,40]. The slope method requires a linear fitting of measured $R_{\text{tot, f}} - R_{\text{tot,b}}$ against film thickness. The slope of the fit represents the reciprocal of the intrinsic cross-plane thermal conductivity ($1/\lambda_{\perp}$). This method by default assumes that R_{C} (including $R_{\text{c,p-f}}$ and $R_{\text{c,f-b}}$) remains identical across measurements of samples with different thicknesses.

However, this underlying assumption of identical R_{C} may not hold true and could lead to significant errors, particularly when the sensor and film specimens have uneven surfaces. Our results demonstrate that such errors can easily reach a value of 26%. Additionally, systematic errors arise from the assumption of 1D heat conduction across the film specimen [38,41], which has not been investigated and quantified with regard to the slope method. Therefore, determining $\lambda_{\perp}$ of thin films with the TPS method is currently associated with considerable uncertainties.

In this work, high-density polyethylene (HDPE) and polypropylene (PP), two polymers with distinct thermal and mechanical properties, were primarily investigated. Additionally, poly(3-hexylthiophene) (P3HT), which has lately attracted significant interest in the context of energy conversion, was also measured. These materials were characterized using TPS measurements under varying measurement conditions, including changes in mounting force and the application of a thermal interface material (TIM). We found that the thermal contact resistance varied with film thickness, which differed from the assumption underlying the slope method and led to considerable deviations. However, using a thermal interface material effectively enhanced the measurements by reducing the variation in thermal contact resistance. In addition, the systematic error and reproducibility of the measurements were carefully evaluated.

2 Experiment

2.1 Materials. HDPE (547999, weight-average molecular weight (M_{W}) = 95 kg/mol, polydispersity index (PDI) = 5.3) and isotactic PP (427888, M_{W} = 250 kg/mol, PDI = 3.7) were obtained from Sigma-Aldrich, St. Louis, MO, and used as received. In addition, P3HT was obtained from Ossila, UK (M1010, M_{W} = 74 kg/mol, PDI = 2.1, regio-regularity = 97%) and used as received.

2.2 Sample Preparation. Free-standing polymer films were fabricated by hot pressing, using a laboratory press (LabPro 200) supplied by Fontijne Presses, the Netherlands, together with a

constant thickness film maker from Specac Ltd., Sheffield, UK. The press applied a force of 15 kN at temperatures that exceeded the melting temperature of the materials: 180°C for HDPE, 210°C for PP, and 290°C for P3HT. The hot-pressed films were subsequently cooled to room temperature at a rate of approximately 40°C/min. The thicknesses of the hot-pressed films were measured using a micrometer with a precision of 1 μm. Bulk polymer samples for reference measurements were hot pressed into cylindrical shapes with a thickness of 4 mm and a radius of 15 mm.

2.3 Pressure Distribution Tests. Prior to the TPS measurements of films, pressure distribution tests were conducted to assess the contact between the experimental components [42], such as background materials, the probe, and the film specimens. In this test, a pair of Prescale Films (i.e., pressure-sensitive films, including A-film and C-film) supplied by Fujifilm, Japan, was placed between the components to study the contact between them. A mounting force of 500 N was applied to the components and Prescale Films for 5 min. A-film is coated with a micro-encapsulated color-forming material, while the C-film is coated with a color-developing material. When used in pairs, these films respond to applied pressure by producing a red color at the point of contact. The intensity of the color correlates with the amount of pressure applied.

2.4 Thermal Conductivity Measurements. The TPS measurements of the film specimens were conducted using a TPS 2200 Thermal Constants Analyzer obtained from Hot Disk AB, Sweden. The probe utilized in the measurements had an effective radius of 11 mm and a 25 μm thick polyimide insulation layers on both sides (model 7854, Fig. 1(*a*)). The background material used was a stainless steel block with a thermal conductivity of 13.5 W/(m · K). A compression stand obtained from Hot Disk was employed for applying a mounting force of up to 550 N. Background measurements were conducted for each level of mounting force.

De-ionized water and silicone oil were employed as a TIM. The de-ionized water, supplied by Sigma-Aldrich, had a thermal conductivity of 0.59 W/(m · K) at room temperature. The silicone oil, sourced from Thermo Fisher Scientific, Waltham, MA, had a thermal conductivity of 0.14 W/(m · K) at room temperature. When using de-ionized water as a TIM, three repeated measurements were conducted within 1 h to avoid the influence of water evaporation. Optionally, sealing the gap between the two background materials with waterproof tape can effectively reduce the evaporation rate.

Two types of reference measurements were carried out: TPS measurements of bulk polymer samples and TWA measurements of pressed polymer films. These methods were selected because they are widely used and supported by international standards [30,31]. TPS measurements of bulk polymers used a sensor with a radius of 3.2 mm (model 5501), while TWA measurements of pressed polymer films employed an Ai-Phase Mobile M3 instrument supplied by Ai-Phase Co., Ltd., Tokyo, Japan.

2.5 Differential Scanning Calorimetry (DSC) Measurements. The specific heat capacity and melting characteristics of the pressed polymer films, including peak melting temperature (T_m) and enthalpy of melting (ΔH_m), were obtained using a DSC 2 instrument from Mettler Toledo, Columbus, OH. The specific heat capacity at room temperature was;obtained using the Sapphire method, with a heating rate of 2°C/min from 10 °C to 40°C. The melting characteristics were obtained from the first heating thermograms with a heating rate of 10°C/min from 20°C to 250°C.

2.6 Simulations. The heat transfer in solids module in COMSOL MULTIPHYSICS (version: 6.1) was utilized to study heat conduction in the TPS measurement setup.

3 Results and Discussion

3.1 Properties of Hot-Pressed Films and Bulk Samples. T_m and ΔH_m of the hot-pressed films were extracted from first heating DSC thermograms (Fig. 1(*a*) available in the Supplemental Materials on the ASME Digital Collection). The crystallinity (X_c) is calculated according to $(\Delta H_m/\Delta H_f^0) \times 100\%$, where ΔH_f^0 is the enthalpy of fusion. The crystallinity of the HDPE and PP films was determined to be 61% and 50%, respectively. The measured ΔH_m of P3HT agrees with the literature values [43]. More details are provided in Table 1 available in the Supplemental Materials.

The hot-pressed films had an average thickness ($\bar{t}$) varying from approximately 40 μm to 400 μm, across 12 distinct thickness levels. The coefficient of variation (CV) in thickness was calculated according to $CV = (\sigma/\bar{t}) \times 100\%$, where σ is the standard deviation of the five measured values taken at different locations on a single specimen. CV was then employed to quantify the flatness of the films (Fig. 1(*b*) available in the Supplemental Materials). Most films displayed a coefficient of variation lower than 3%, though films thinner than 80 μm showed higher variations.

The thermal conductivity of hot-pressed films determined by TWA ($\lambda_{\perp,TWA}$) was 0.488 ± 0.049 W/(m · K) for HDPE and 0.247 ± 0.025 W/(m · K) for PP. These values represent one of the two sets of reference values used in this study.

Another set of reference thermal conductivity values was derived using TPS measurements of bulk polymer samples (Table 1), where the thermal conductivity ($\lambda_{bulk,\ TPS}$) was 0.465 ± 0.023 W/(m · K) for HDPE and 0.269 ± 0.013 W/(m · K) for PP. The two sets of reference values are in good agreement, in particular when considering differences in sample preparation, with recorded differences of less than 8%. Additionally, these two sets of reference values fall within the range of thermal conductivity values reported in the literature: 0.42 W/(m · K) to 0.52 W/(m · K) for HDPE [44–46] and 0.22 W/(m · K) to 0.27 W/(m · K) for PP [47–49].

3.2 Pressure Distribution. Six pressure distribution tests with different arrangements of components were conducted. To assess the contact between two blocks of the background material, the first test was set up with an arrangement from the top to bottom comprising background material, Prescale Films, and background material (abbreviated as BG–Prescale Films–BG). The second test used an arrangement of BG–probe–Prescale Films–BG to study the contact between the probe and the background material. The remaining tests focused on the contact between film specimens

Table 1 Material properties

Material	λ (W/(m · K))	ρ (kg/m^3)	C_p (J/(kg · K))
HDPE	0.465[a]	950[b]	1923[c]
PP	0.269[a]	900[b]	1613[c]
Background material (stainless steel)	13.5[a]	8150[b]	460[a]
Insulation layer (polyimide)	0.18[d]	1420[e]	1090[e]
Probe (nickel)	91.4[f]	8900[f]	444[f]

[a]Determined by TPS measurements of bulk samples.
[b]Determined from the mass and volume of the samples.
[c]Obtained from the DSC Sapphire method.
[d]Obtained from a background measurement with de-ionized water as the TIM.
[e]Obtained from Ref. [50].
[f]Obtained from Ref. [38].

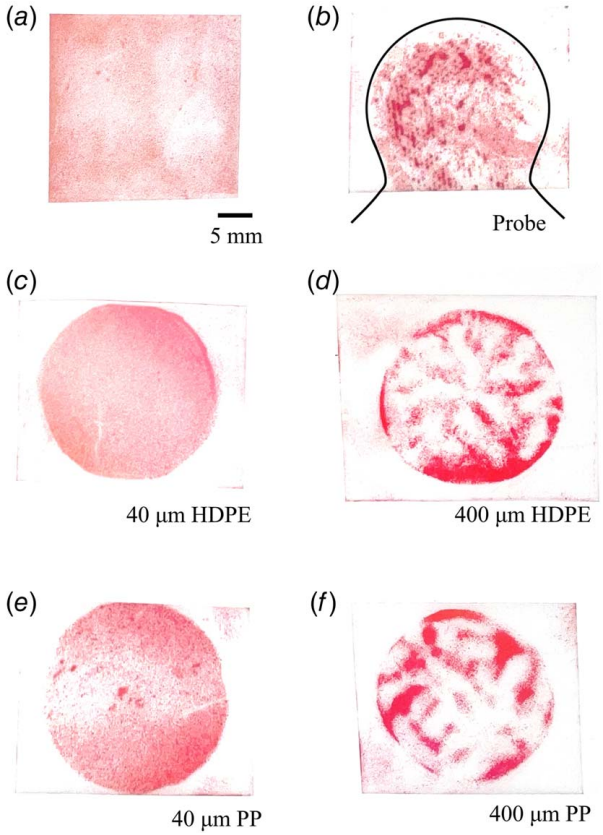

Fig. 3 The results of the pressure distribution test examining the contact between the background material and various components: (*a*) second block of the background material, (*b*) the probe, (c) a 40 μm-thick HDPE film, (*d*) a 400 μm-thick HDPE film, (e) a 40 μm-thick PP film, and (*f*) a 400 μm-thick PP film. The intensity of the coloration is related to the pressure level. To identify the position of the probe, a contour line in (*b*) is provided to represent the outer edge of the probe.

and the background material, using the arrangement BG–film specimen–Prescale Films–BG.

The first experiment showed an even distribution of color (Fig. 3(*a*)), suggesting a uniform pressure distribution between two blocks of the background material. The second experiment involving a probe demonstrated a heterogeneous and irregular coloration, characterized by small clusters of higher intensity (Fig. 3(*b*)). These clusters likely resulted from the bulges in the nickel pattern and polyimide surface, which can be seen in Fig. 1(*a*).

The tests involving a thin-film specimen (approximately 40 μm) displayed a more uniform and consistent color distribution (Figs. 3(*c*) and 3(*e*)). In contrast, thick film specimens (approximately 400 μm) led to a visibly larger and irregularly colored region (Figs. 3(*d*) and 3(*f*)). This irregularity is expected to be caused by the uneven surfaces and the low pliability of the thick films, showing the influence of film thickness on its surface properties.

3.3 Thermal Conductivity From Transient Plane Source Film Measurements

3.3.1 Measurement Without Thermal Interface Material. In the cases where TPS was carried out without a TIM, $\lambda_{\perp,a}$ of both HDPE and PP films (Fig. 4(*a*)) proved lower than the reference values obtained from the TWA and the TPS method for bulk materials (Table 1), which we attribute to the presence of thermal contact resistance. Generally, the thicker specimens displayed a higher apparent cross-plane thermal conductivity. This is because the thicker specimens possess a larger intrinsic thermal resistance ($R_f = \delta/\lambda_\perp$) and thus a larger $R_{tot,f}$, which diminished the influence of thermal contact resistance.

In addition, a higher mounting force led to an increase in the values of $\lambda_{\perp,a}$, particularly in the case of HDPE. This increase is attributed to a reduction in thermal contact resistance with greater mounting force. However, if the specimens are compressible, changes in mounting force may also alter their thickness, which in turn effects their thermal conductivity. Notably, HDPE films thinner than 50 μm exhibited anomalously higher values of $\lambda_{\perp,a}$ at a force of 300 N, likely due to the softer nature of thin HDPE films, which resulted in better contact with the probe and background materials.

Subsequently, we extracted the intrinsic thermal conductivity using the slope method (Fig. 4(*b*)). Data from the films thicker than 80 μm were utilized due to the low uncertainty in the determined thickness (Fig. 1(*b*) available in the Supplemental Materials). $R_{tot,f} - R_{tot,b}$ was initially plotted against the film thickness and fitted with a linear function. The uncertainty in the fit parameters (slope and intercept) was calculated in accordance with the methodology described in Refs. [40,51]. Afterward, $\lambda_\perp$ was obtained as the reciprocal of the slope from these fits (Table 2). Overall, the $\lambda_\perp$values of HDPE and PP were still underestimated, showing a difference of up to 26% and 22%, respectively.

Moreover, the values of $\lambda_\perp$ also changed with the mounting force. When the external mounting force was increased, the $\lambda_\perp$values of HDPE increased by 17% from 0.343 W/(m · K) to 0.411 W/(m · K), while those of PP increased by 9% from 0.209 W/(m · K) to 0.230 W/(m · K). Regardless, the highest values obtained were still significantly lower than reference values of 0.465 W/(m · K) for HDPE and 0.269 W/(m · K) for PP.

In addition, the influence of the mounting force differed with the specimen thickness (Fig. 4(*b*)). $R_{tot,f} - R_{tot,b}$ in the case of thin specimens decreased only slightly with increased mounting force (small arrows), whereas in the case of thicker specimens a more significant decrease was observed (big arrows). This indicates that there is greater potential for reducing R_c in case of thick films by applying a higher mounting force. Additionally, considering the uneven surfaces and reduced pliability of thicker films, we argue that these films tend to result in a higher R_c. This is at odds with the underlying assumptions of the slope method and thus resulted in errors.

A higher R_c in case of thick films leads to a higher total thermal resistance, resulting in a steeper slope of the linear fit and, consequently, a lower value of $\lambda_\perp$. This phenomenon likely contributes to the observed underestimation of the intrinsic thermal conductivity if no thermal interface material is used.

3.3.2 Measurements With Liquid Thermal Interface Material. TPS measurements with water as the TIM yielded higher values of thermal conductivity compared to the previous case without a TIM (Fig. 4(*c*)). The increase in $\lambda_{\perp,a}$ can be attributed to a reduction in thermal contact resistance. Despite this increase, the values of $\lambda_{\perp,a}$ of both HDPE and PP remained lower than their respective reference values, which we attribute to the fact that employing water did not completely eliminate thermal contact resistance.

Similarly, $R_{tot,f} - R_{tot,b}$ was again plotted against specimen thickness (Fig. 4(*d*)) and fitted to calculate $\lambda_\perp$ and the additional thermal contact resistance (intercept). Unlike the scenario without a TIM, the values of $\lambda_\perp$ were more consistent across different mounting forces, with a small difference of around 1% (Table 2). In case of HDPE, average values of $\lambda_\perp$ and the intercept over different mounting forces were 0.450 W/(m · K) and 55 mm^{2}K/W, respectively. In case of PP, average values were 0.277 W/(m · K) and 110 mm^{2}K/W, respectively. These values of $\lambda_\perp$ agreed well with the reference values from TPS measurements on bulk materials (Table 1) and the TWA method, differing by less than 4% and 11%, respectively.

Analogous measurements with a mounting force of 50 N were conducted using silicone oil as the TIM (Figs. 5(*a*) and 5(*b*)). In

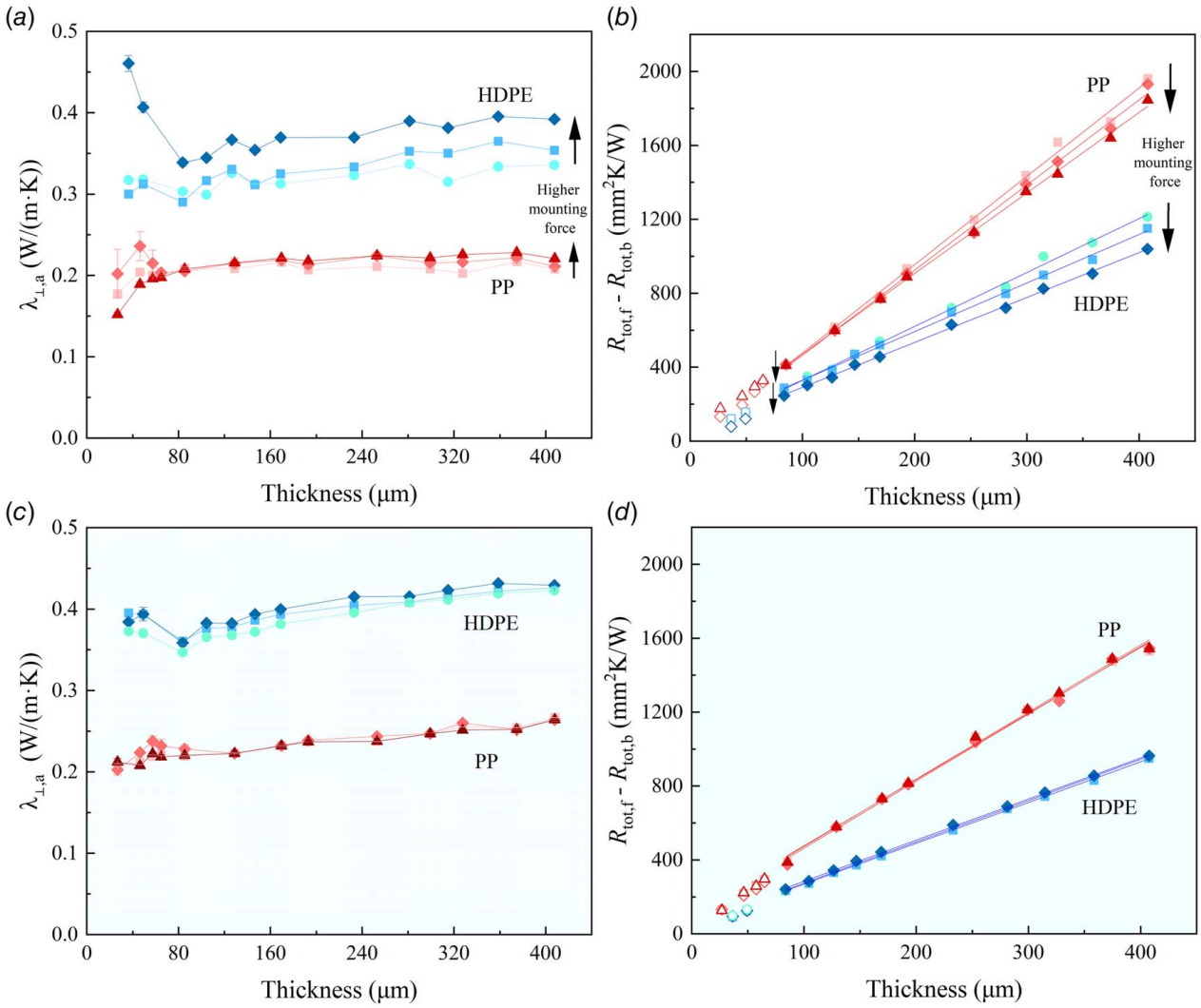

Fig. 4 Results of the TPS measurements of HDPE and PP films (mounting force: ● 0 N, ■ 50 N, ◆ 300 N, ▲ 550 N): (*a*) the values of the apparent thermal conductivity versus the film thickness, obtained from the measurements without a TIM; (*b*) $R_{tot,f} - R_{tot,b}$ as a function of the film thickness, along with linear fits. Data points from the specimens thinner than 80 μm (open symbols) were excluded from the fitting; (*c*) the values of the apparent thermal conductivity versus film thickness, obtained from the measurements using water as the TIM; (*d*) $R_{tot,f} - R_{tot,b}$ versus film thickness, along with the linear fits. Data points from specimens thinner than 80 μm (open symbols) were excluded from the fitting.

this case, $\lambda_\perp$ of HDPE and PP was calculated to be 0.435 W/(m · K) and 0.264 W/(m · K), respectively, similar to values obtained from the measurements with water as the TIM. Due to the low volatility of silicone oil, a high measurement stability was achieved. Specifically, the measurement results obtained for HDPE films under a mounting force of 500 N remained exceptionally stable for over 10 days, with an observed fluctuation of less than 0.5% (Fig. 5(*c*)). This also implies that the influence of creep is negligible in our measurements. However, the removal of silicone oil from the specimens at the end of measurement is normally more difficult compared to that of de-ionized water.

Table 2 The results from the slope method, including $\lambda_\perp$ (reciprocal of slope) and the additional thermal contact resistance (intercept)

Material	Mounting force (N)	$\lambda_\perp$(W/(m · K)) (without TIM)	Intercept (mm²K/W) (without TIM)	$\lambda_\perp$(W/(m · K)) (with water as TIM)	Intercept (mm²K/W) (with water as TIM)
HDPE	0	0.343 ± 0.007.	37.5 ± 14.5	0.447 ± 0.003	50.6 ± 4.1
	50	0.381 ± 0.007	67.3 ± 12.2	0.453 ± 0.003	48.5 ± 3.6
	300	0.411 ± 0.005	48.0 ± 7.7	0.449 ± 0.004	61.6 ± 4.5
PP	50	0.209 ± 0.005	0.2 ± 28.4	0.279 ± 0.007	118.3 ± 25.7
	300	0.217 ± 0.005	4.3 ± 25.8	0.276 ± 0.007	100.9 ± 24.0
	550	0.230 ± 0.003	35.6 ± 16.2	0.275 ± 0.007	110.0 ± 23.2

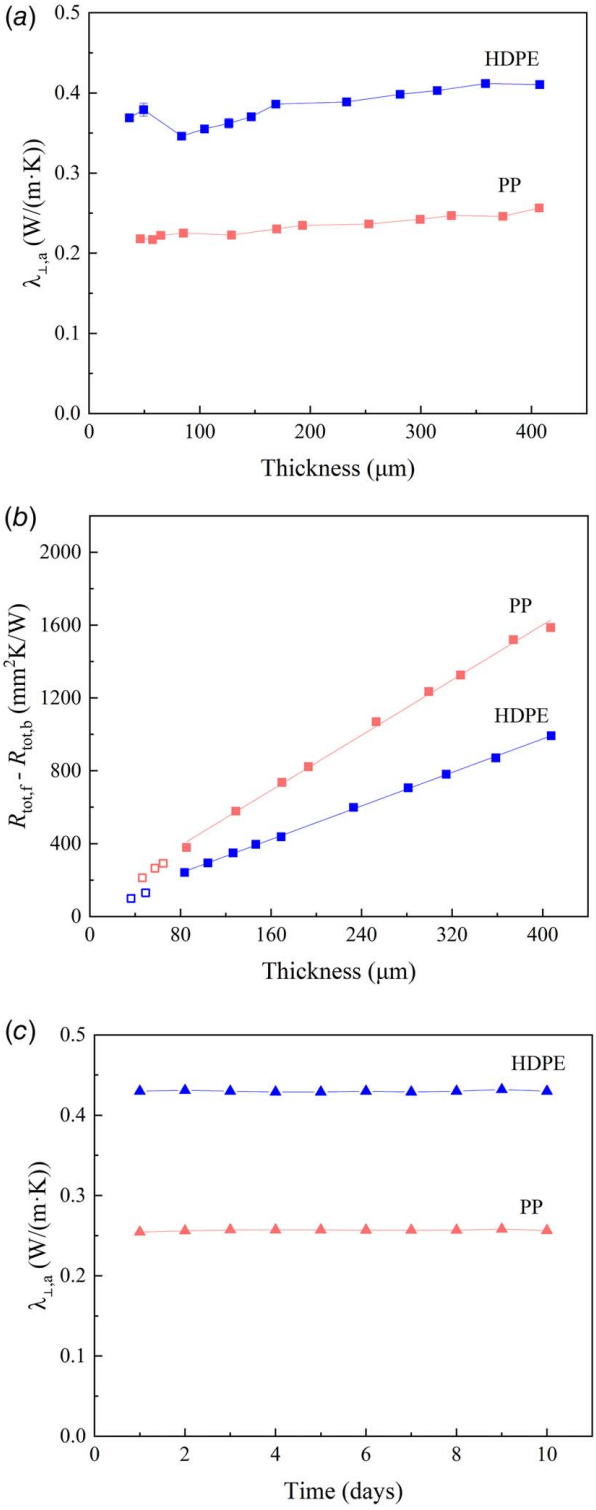

Fig. 5 Measurement results for HDPE and PP using silicone oil as the thermal interface material: (*a*) the values of $\lambda_{\perp,a}$ versus the film thickness for a mounting force of 50 N (■); (*b*) $R_{tot,f} - R_{tot,b}$ versus the film thickness for a mounting force of 50 N, along with linear fits. The data points from the specimens thinner than 80 μm (outlier open symbols) were excluded from the fitting; and (c) the values of $\lambda_{\perp,a}$ of 400 μm-thick HDPE and PP films versus time for a mounting force of 500 N (▲)

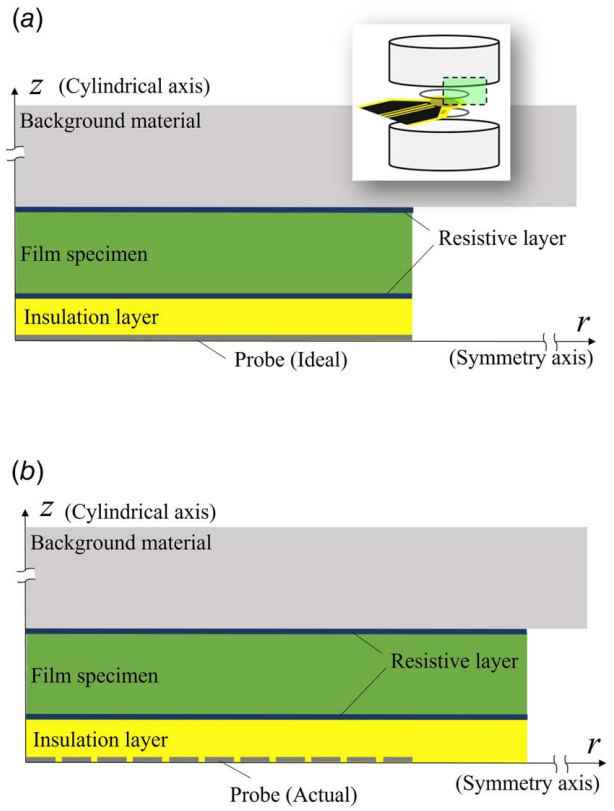

Fig. 6 Schematic depicting the two simulation models of TPS measurements involving de-ionized water that represent (*a*) the ideal and (*b*) the actual scenarios. The dashed frame in the inset indicates the computational domain.

3.4 Simulation. To investigate the systematic error caused by the assumption of 1D heat flow across the specimen, two simulation models were developed. Considering the axisymmetric heat conduction in the measurements, the models were reduced to two dimensions (2D) to improve computational efficiency [52,53]. The development of the 2D models relied on several key assumptions:

- The measurement setup, including the probe, background material, layers, and interfaces can be treated as axisymmetric.
- The bifilar probe can be approximated as a series of concentric and uniformly spaced ring sources.
- Heat transfer between the measurement components and the ambient environment is considered negligible (adiabatic boundary condition).
- Heat transfer via convection and radiation is considered negligible.
- Material properties are assumed to remain constant during the measurement.

One simulation model was developed to represent the ideal scenario where heat flow across the film specimen and the insulation layer is 1D (ideal scenario, Fig. 6(*a*)). In this model, an ideal heat source was depicted as a thin rectangle, transformable into a circular probe by rotation around the origin. The radius of the specimen layer, TIM layers, and insulation layers was set to be the same as the equivalent radius of the probe (11 mm).

The second model simulated the conditions of the actual measurements (Fig. 6(*b*)). A series of uniformly spaced thin rectangles with a height of 5 μm and a width of 800 μm was utilized to represent the double spiral probe. The space between the rectangles was 200 μm. In addition, the radius of the specimen and insulation layers was set to be 3 mm larger than that of the probe, consistent with the experimental setup.

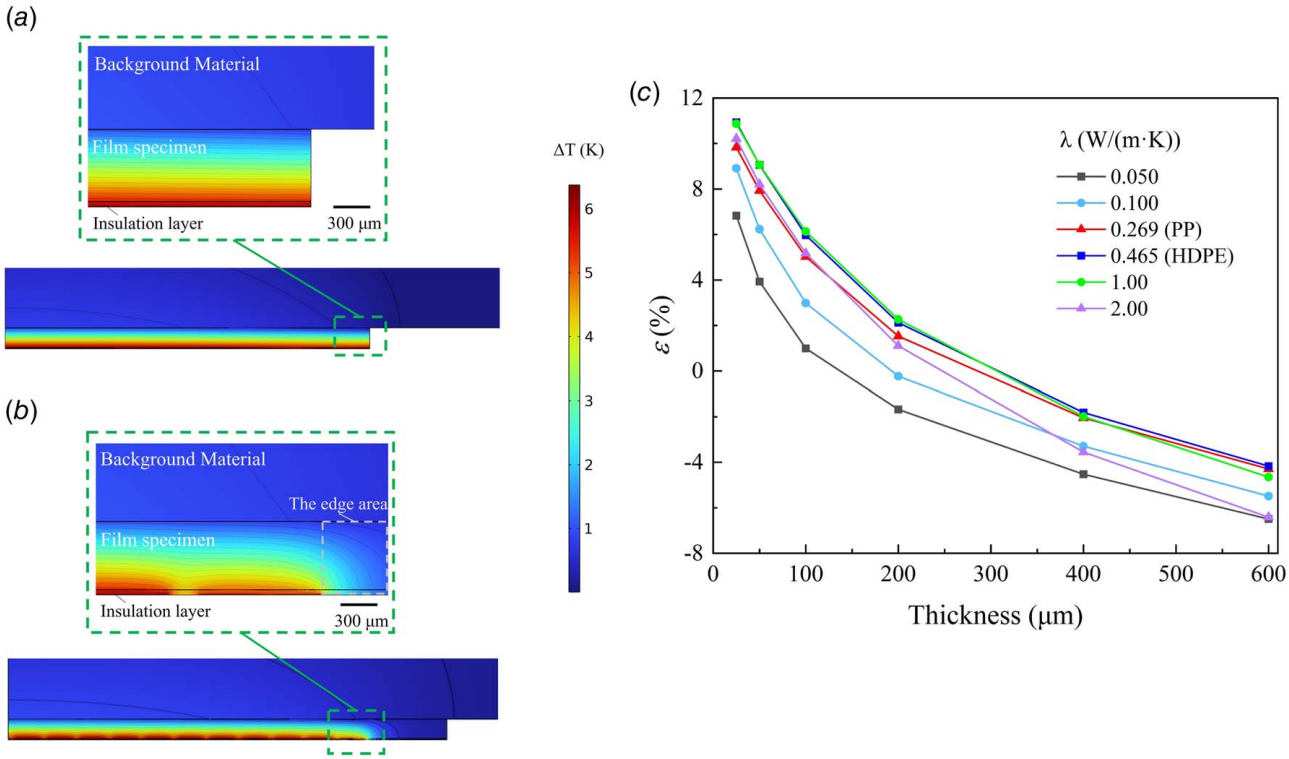

Fig. 7 Comparison of temperature distribution across the film specimen at the end of the measurement period (20 s) between the (*a*) ideal and (*b*) actual scenarios; and (c) difference in $R_{tot,f} - R_{tot,b}$ between the ideal and actual scenarios

The governing equations for heat conduction in the simulation are

$$\rho C_p \frac{\partial T}{\partial t} + \nabla q = Q \tag{8}$$

$$q = -\lambda \nabla T \tag{9}$$

where q is the heat flux by conduction and Q is the power supplied by the heat source. Thermal contact resistance in measurements using a TIM was considered and represented by equivalent thin resistive layers in the simulation model. The resistance of each layer was set to 28 mm^2K/W for HDPE measurements and 55 mm^2K/W for PP measurements, corresponding to half of the intercept obtained from the slope method (Table 2). The heating power and heating time of the probe were set to 1 W and 20 s, respectively, to align with the experimental conditions. The material properties, including λ, density (ρ), and the specific heat capacity (C_p), are listed in Table 1.

We first compare the simulated temperature distribution between the ideal and actual scenarios. In the ideal scenario, the isotherms are parallel within the film specimen, suggesting 1D heat conduction (Fig. 7(*a*)). However, in the actual scenario (Fig. 7(*b*)), the temperature distribution differs from the ideal scenario due to two factors. First, the actual double spiral probe has a slightly smaller heating area compared to an ideal circular probe with the same radius, which tends to result in a higher average temperature increase and thus an underestimated value of the thermal conductivity. Second, the radius of the insulation layer and the film specimen is slightly larger than that of the probe, which tends to create an additional edge area allowing heat to be conducted to the background material. This causes a lower average temperature increase, which results in an overestimation of $\lambda_\perp$.

The difference in $R_{tot,f} - R_{tot,b}$ between the ideal and actual scenarios (ϵ) was calculated according to

$$\epsilon = \left[\frac{(R_{tot,f} - R_{tot,b})_{act}}{(R_{tot,f} - R_{tot,b})_{idl}} - 1 \right] \times 100\% \tag{10}$$

where the subscript *idl* and *act* denote the ideal and actual scenarios, respectively. For a given sensor radius (11 mm in this case), ϵ varies depending on both the thickness and the thermal conductivity of the film specimens (Fig. 7(*c*)). In case of HDPE and PP, ϵ remains below 7% over the thickness range of 80–400 μm. Note that these values of ϵ will vary when a sensor with a different radius is utilized.

For thinner film specimens, the smaller area of the actual probe (the first factor) has a more pronounced effect, leading to an underestimated value of $\lambda_\perp$. This factor poses another challenge in evaluating thinner film specimens, alongside the aforementioned uncertainty in thickness determination. On the other hand, in case of thicker specimens, the influence of the additional edge area (the second factor) becomes more significant, resulting in an overestimated value of $\lambda_\perp$.

These systematic measurement errors at each thickness can accumulate and propagate into the final thermal conductivity value determined by the slope method. With knowledge of ϵ, the measured values of $R_{tot,f} - R_{tot,b}$ (Fig. 4(*d*)) were first adjusted and used to recalculate the thermal conductivity. By comparing the previous and recalculated thermal conductivity values (Table 2 available in the Supplemental Materials), the accumulated systematic errors were determined to be 4% for HDPE and 5% for PP.

To further reduce systematic errors, three general modifications to the probe are proposed so that the heat conduction during the measurement more closely resembles the ideal scenario: (1) increase of the probe radius, (2) narrowing of the gap within the double spiral, and (3) reduction of the thickness of the polyimide insulation layers.

3.5 Influence of Specimen Number. This section discusses the influence of the number of specimens (with different

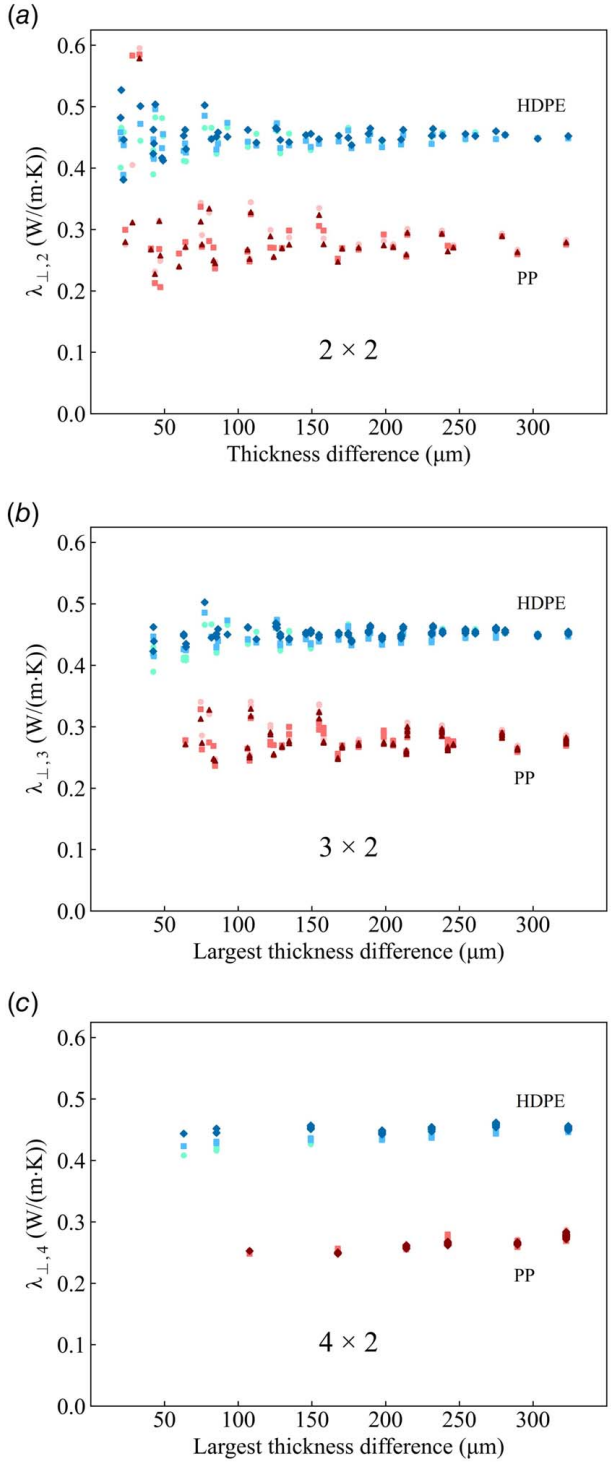

Fig. 8 Variation in $\lambda_{\perp}$ of HDPE and PP as a function of thickness difference for different mounting forces (● 0 N, ■ 50 N, ◆ 300 N, ▲ 550 N), across various systems: (*a*) 2 × 2, (*b*) 3 × 2, and (*c*) 4 × 2 datasets

thicknesses), providing insights into the reproducibility, and robustness of the TPS measurements when water is used as the TIM.

First, the intrinsic thermal conductivity calculated using only two pairs (2 × 2) of film specimens ($\lambda_{\perp,2}$) was examined. To achieve this, subsets of data from 2 × 2 specimens were extracted from Fig. 4(*d*) (solid symbols). For every subset, a linear regression was carried out, from which the slope and $\lambda_{\perp,2}$ were obtained. Subsequently, $\lambda_{\perp,2}$ values were plotted against the thickness difference between the 2 × 2 specimens (Fig. 8(*a*)).

Table 3 Comparison of $\lambda_{\perp}$ and standard deviation obtained from datasets with varying specimen numbers

Thermal conductivity (W/(m · K))	$\lambda_{\perp,2}$	$\lambda_{\perp,3}$	$\lambda_{\perp,4}$
HDPE	0.448 ± 0.022	0.448 ± 0.012	0.446 ± 0.008
PP	0.289 ± 0.065	0.278 ± 0.019	0.269 ± 0.009

First of all, the values of $\lambda_{\perp,2}$ were seen to evenly scatter across different mounting forces, indicating no dependence on the mounting force. In addition, the values of $\lambda_{\perp,2}$ were more scattered when the thickness difference was small. As the thickness difference increased, the values became more consistent. Overall, the standard deviation of $\lambda_{\perp,2}$ was 0.022 W/(m · K) (5%) for HDPE and 0.065 W/(m · K) (22%) for PP.

When the thickness difference was larger than 200 μm, the standard deviation significantly decreased to 0.006 W/(m · K) (1%) for HDPE and 0.013 W/(m · K) (5%) for PP. This suggests that 2 × 2 specimens with a significant thickness difference are likely sufficient for obtaining viable results of low uncertainty.

The intrinsic thermal conductivity obtained from 3 × 2 film specimens ($\lambda_{\perp,3}$) was also analyzed (Fig. 8(*b*)). With an additional specimen pair, the values of $\lambda_{\perp,3}$ were observed to be more consistent when the thickness difference was small, especially in the case of PP specimens. In case of both HDPE and PP, the standard deviation is less than 0.02 W/(m · K). Lastly, the intrinsic thermal conductivity from subsets with 4 × 2 specimens ($\lambda_{\perp,4}$) was evaluated (Fig. 8(*c*)). Differing from the preceding scenarios, the values of $\lambda_{\perp,4}$ in this case showed a much smaller standard deviation, especially when the thickness difference was small. Specifically, the standard deviation was 0.008 W/(m · K) (2%) for HDPE and 0.009 W/(m · K) (3%) for PP. All the results are summarized in Table 3.

Based on this analysis, two sets of specimens are recommended for precise TPS measurements with a standard deviation less of than 0.02 W/(m · K). The first set includes 2 × 2 specimens, each thicker than 80 μm, with a thickness difference exceeding 200 μm. The second set consists of 4 × 2 specimens, each thicker than 80 μm.

To illustrate the utility of the here proposed specimen set, 2 × 2 P3HT films with a thickness difference of over 200 μm were also measured, which gave an intrinsic cross-plane thermal conductivity of 0.296 ± 0.030 W/(m · K). This value is comparable to the thermal conductivity of P3HT films or bulk material prepared by other methods, such as drop casting (0.21 W/(m · K)) [54], spin coating (0.27 W/(m·K)) [55], cold pressing (0.19 W/(m · K)) [56], and drop casting followed by a cold pressing (0.33 W/(m · K)) [57].

4 Conclusions

In our measurements, thicker films led to a larger thermal contact resistance, likely due to their comparatively uneven surfaces and low pliability. This is at odds with the fundamental assumption of the slope method that heat conduction across the film is one-dimensional, leading to significant errors of up to 26% in case of HDPE. To address this issue, liquid thermal interface materials, e.g., de-ionized water or silicone oil, were introduced. The liquid thermal interface material ensured a consistent and low thermal contact resistance independent of film thickness, which enabled the precise extraction of the intrinsic cross-plane thermal conductivity. The extracted values for HDPE and PP agreed well with reference values, with a difference of 4%. This level of accuracy is comparable to the typical accuracy of 5% achieved by the LFA method for millimeter-thick samples.

Moreover, finite-element simulations were performed to quantify systematic errors arising from the assumption of one-dimensional heat conduction across the film specimens. The results indicate that the systematic error in the thermal conductivity of HDPE and

PP, determined via the slope method, is less than 5%. In addition, the simulations imply that samples with a thermal conductivity as low as 0.05 W/(m · K) and as high as 2 W/(m · K) can also be measured with a small error.

Finally, we observed that both the number of specimens and the thickness difference among them influence the overall precision of the measured intrinsic conductivity. Using as few as two specimens, provided they have sufficiently different thicknesses, can yield precise results with a standard deviation below 0.02 W/(m · K).

Hence, we propose a refined measurement procedure for efficient and reliable characterization of film specimens. The refined procedure involves the measurement of at least two sets of specimens with a significant thickness difference, application of a liquid thermal interface material (e.g., de-ionized water) to ensure a consistent and low thermal contact resistance, and subsequent use of the slope method to extract the intrinsic cross-plane thermal conductivity. In the future, it would be worthwhile to explore alternative liquid TIMs such as ethylene glycol for measurements under varying conditions.

Acknowledgment

This project has received funding from the European Union's Horizon 2020 research and innovation program under the Marie Skłodowska-Curie grant agreement No. 955837. The authors also wish to thank Dr. Silas Gustafsson for his insightful comments and Dr. Henrik Otterberg for his thorough language review.

Data Availability Statement

The datasets generated and supporting the findings of this article are obtainable from the corresponding author upon reasonable request.

References

[1] McKeen, L. W., 2017, *Film Properties of Plastics and Elastomers*, Elsevier, Amsterdam, The Netherlands.
[2] Tritt, T. M., 2005, *Thermal Conductivity: Theory, Properties and Applications*, Springer, Berlin, Germany.
[3] Yang, X., Liang, C., Ma, T., Guo, Y., Kong, J., Gu, J., Chen, M., and Zhu, J., 2018, "A Review on Thermally Conductive Polymeric Composites: Classification, Measurement, Model and Equations, Mechanism and Fabrication Methods," Adv. Compos. Hybrid Mater., **1**(2), pp. 207–230.
[4] Rao, Z., and Wang, S., 2011, "A Review of Power Battery Thermal Energy Management," Renew. Sustain. Energy Rev., **15**(9), pp. 4554–4571.
[5] Karimi, G., Li, X., and Teertstra, P., 2010, "Measurement of Through-Plane Effective Thermal Conductivity and Contact Resistance in PEM Fuel Cell Diffusion Media," Electrochim. Acta, **55**(5), pp. 1619–1625.
[6] Kandlikar, S. G., and Lu, Z., 2009, "Thermal Management Issues in a PEMFC Stack–A Brief Review of Current Status," Appl. Therm. Eng., **29**(7), pp. 1276–1280.
[7] Wang, Y., Yang, L., Shi, X.-L., Shi, X., Chen, L., Dargusch, M. S., Zou, J., and Chen, Z.-G., 2019, "Flexible Thermoelectric Materials and Generators: Challenges and Innovations," Adv. Mater., **31**(29), p. 1807916.
[8] Masoumi, S., O'Shaughnessy, S., and Pakdel, A., 2022, "Organic-Based Flexible Thermoelectric Generators: From Materials to Devices," Nano Energy, **92**, p. 106774.
[9] Xu, Y., Kraemer, D., Song, B., Jiang, Z., Zhou, J., Loomis, J., Wang, J., et al., 2019, "Nanostructured Polymer Films With Metal-Like Thermal Conductivity," Nat. Commun., **10**(1), p. 1771.
[10] Ronca, S., Igarashi, T., Forte, G., and Rastogi, S., 2017, "Metallic-Like Thermal Conductivity in a Lightweight Insulator: Solid-State Processed Ultra High Molecular Weight Polyethylene Tapes and Films," Polymer, **123**, pp. 203–210.
[11] Rodgers, P., Eveloy, V., Diana, A., Darawsheh, I., and Almaskari, F., 2017, "Mechanical and Heat Transfer Performance Investigation of High Thermal Conductivity, Commercially Available Polymer Composite Materials for Heat Exchange in Electronic Systems," ASME J. Therm. Sci. Eng. Appl., **9**(3), p. 031008.
[12] Zhao, D., Qian, X., Gu, X., Jajja, S. A., and Yang, R., 2016, "Measurement Techniques for Thermal Conductivity and Interfacial Thermal Conductance of Bulk and Thin Film Materials," ASME J. Electron Packag., **138**(4), p. 040802.
[13] Jiang, P., Qian, X., and Yang, R., 2018, "Tutorial: Time-Domain Thermoreflectance (TDTR) for Thermal Property Characterization of Bulk and Thin Film Materials," J. Appl. Phys., **124**(16), p. 161103.
[14] Capinski, W., Maris, H., Ruf, T., Cardona, M., Ploog, K., and Katzer, D., 1999, "Thermal-Conductivity Measurements of GaAs/AlAs Superlattices Using a Picosecond Optical Pump-and-Probe Technique," Phys. Rev. B, **59**(12), p. 8105.
[15] Schmidt, A. J., Cheaito, R., and Chiesa, M., 2009, "A Frequency-Domain Thermoreflectance Method for the Characterization of Thermal Properties," Rev. Sci. Instrum., **80**(9), p. 094901.
[16] Schmidt, A. J., Chen, X., and Chen, G., 2008, "Pulse Accumulation, Radial Heat Conduction, and Anisotropic Thermal Conductivity in Pump-Probe Transient Thermoreflectance," Rev. Sci. Instrum., **79**(11), p. 114902.
[17] Xu, K., Guo, J., Raciti, G., Goni, A. R., Alonso, M. I., Borrise, X., Zardo, I., Campoy-Quiles, M., and Reparaz, J. S., 2023, "In-Plane Thermal Diffusivity Determination Using Beam-Offset Frequency-Domain Thermoreflectance With a One-Dimensional Optical Heat Source," Int. J. Heat Mass Transfer, **214**, p. 124376.
[18] Min, S., Blumm, J., and Lindemann, A., 2007, "A New Laser Flash System for Measurement of the Thermophysical Properties," Thermochim. Acta, **455**(1–2), pp. 46–49.
[19] ISO 22007-4:2024, Plastics – Determination of Thermal Conductivity and Thermal Diffusivity.
[20] Abad, B., Borca-Tasciuc, D.-A., and Martin-Gonzalez, M., 2017, "Non-Contact Methods for Thermal Properties Measurement," Renew. Sustain. Energy Rev., **76**, pp. 1348–1370.
[21] Craddock, J. D., Burgess, J. J., Edrington, S. E., and Weisenberger, M. C., 2017, "Method for Direct Measurement of On-Axis Carbon Fiber Thermal Diffusivity Using the Laser Flash Technique," ASME J. Therm. Sci. Eng. Appl., **9**(1), p. 014502.
[22] Yang, J., Ziade, E., and Schmidt, A. J., 2016, "Uncertainty Analysis of Thermoreflectance Measurements," Rev. Sci. Instrum., **87**(1), p. 014901.
[23] Pérez, L. A., Xu, K., Wagner, M. R., Dörling, B., Perevedentsev, A., Goñi, A. R., Campoy-Quiles, M., Alonso, M. I., and Reparaz, J. S., 2022, "Anisotropic Thermoreflectance Thermometry: A Contactless Frequency-Domain Thermoreflectance Approach to Study Anisotropic Thermal Transport," Rev. Sci. Instrum., **93**(3), p. 034902.
[24] Qian, X., Ding, Z., Shin, J., Schmidt, A. J., and Chen, G., 2020, "Accurate Measurement of In-Plane Thermal Conductivity of Layered Materials Without Metal Film Transducer Using Frequency Domain Thermoreflectance," Rev. Sci. Instrum., **91**(6), p. 064903.
[25] Zhu, J., Tang, D., Wang, W., Liu, J., Holub, K. W., and Yang, R., 2010, "Ultrafast Thermoreflectance Techniques for Measuring Thermal Conductivity and Interface Thermal Conductance of Thin Films," J. Appl. Phys., **108**(9), p. 094315.
[26] Zhao, Y.-H., Wu, Z.-K., and Bai, S.-L., 2016, "Thermal Resistance Measurement of 3D Graphene Foam/Polymer Composite by Laser Flash Analysis," Int. J. Heat Mass Transfer, **101**, pp. 470–475.
[27] ISO 8302:1991. Thermal Insulation – Determination of Steady-State Thermal Resistance and Related Properties – Guarded Hot Plate Apparatus.
[28] Cahill, D. G., 1990, "Thermal Conductivity Measurement From 30 to 750 K: The 3ω Method," Rev. Sci. Instrum., **61**(2), pp. 802–808.
[29] Dames, C., 2013, "Measuring the Thermal Conductivity of Thin Films: 3 Omega and Related Electrothermal Methods," Annu. Rev. Heat Transf., **16**(16), pp. 7–44.
[30] ISO 22007-3:2008. Plastics – Determination of Thermal Conductivity and Thermal Diffusivity – Part 3: Temperature Wave Analysis Method.
[31] ISO 22007-2:2022. Plastics – Determination of Thermal Conductivity and Thermal Diffusivty – Part 2: Transient Plane Heat Source (Hot Disc) Method.
[32] Hashimoto, T., Matsui, Y., Hagihara, A., and Miyamoto, A., 1990, "Thermal Diffusivity Measurement of Polymer Films by the Temperature Wave Method Using Joule-Heating," Thermochim. Acta, **163**, pp. 317–324.
[33] Gustafsson, S. E., 1991, "Transient Plane Source Techniques for Thermal Conductivity and Thermal Diffusivity Measurements of Solid Materials," Rev. Sci. Instrum., **62**(3), pp. 797–804.
[34] Wereszczak, A. A., Emily Cousineau, J., Bennion, K., Wang, H., Wiles, R. H., Burress, T. B., and Wu, T., 2017, "Anisotropic Thermal Response of Packed Copper Wire," ASME J. Therm. Sci. Eng. Appl., **9**(4), p. 041006.
[35] Gustavsson, M., and Hälldahl, L., 2006, "Thermal Conductivity Measurements of Thin Insulating Layers Deposited on High-Conducting Sheets," Int. J. Thermophys., **27**(1), pp. 195–208.
[36] Gustavsson, J., Gustavsson, M., and Gustafsson, S., 1999, "On the Use of the Hot Disk Thermal Constants Analyser for Measuring the Thermal Conductivity of thin Samples of Electrically Insulating Materials," Thermal Conductivity, Vol. **24**, pp. 116–122.
[37] Instruction Manual, 2022. *Hot Disk Thermal Constants Analyser*, Hot Disk AB, Sweden.
[38] Zhang, H., Li, M.-J., Fang, W.-Z., Dan, D., Li, Z.-Y., and Tao, W.-Q., 2014, "A Numerical Study on the Theoretical Accuracy of Film Thermal Conductivity Using Transient Plane Source Method," Appl. Therm. Eng., **72**(1), pp. 62–69.
[39] Feng, B., Zhang, Y.-H., Tu, J., Fan, L.-W., and Yu, Z.-T., 2022, "Determination on the Thermal Conductivity and Thermal Contact Resistance of Thin Composite Phase Change Films as a Thermal Interfacial Material," Case Stud. Therm. Eng., **33**, p. 101979.
[40] Ahadi, M., Andisheh-Tadbir, M., Tam, M., and Bahrami, M., 2016, "An Improved Transient Plane Source Method for Measuring Thermal Conductivity of Thin Films: Deconvoluting Thermal Contact Resistance," Int. J. Heat Mass Transfer, **96**, pp. 371–380.
[41] Landry, D., Flores, R., and Goodman, R. B., 2024, "Estimating the Thermal Conductivity of Thin Films: A Novel Approach Using the Transient Plane Source Method," ASME J. Heat Transfer-Trans. ASME, **146**(3), p. 031004.
[42] Bachus, K. N., DeMarco, A. L., Judd, K. T., Horwitz, D. S., and Brodke, D. S., 2006, "Measuring Contact Area, Force, and Pressure for Bioengineering

Applications: Using Fuji Film and Tekscan Systems," Med. Eng. Phys., **28**(5), pp. 483–488.
[43] Koch, F. P. V., Rivnay, J., Foster, S., Müller, C., Downing, J. M., Buchaca-Domingo, E., Westacott, P., et al., 2013, "The Impact of Molecular Weight on Microstructure and Charge Transport in Semicrystalline Polymer Semiconductors-Poly (3-hexylthiophene), A Model Study," Prog. Polym. Sci., **38**(12), pp. 1978–1989.
[44] Cardarelli, F., 2008, *Materials Handbook: A Concise Desktop Reference*, Springer, Berlin, Germany.
[45] Ye, C.-M., Shentu, B.-Q., and Weng, Z.-X., 2006, "Thermal Conductivity of High Density Polyethylene Filled With Graphite," J. Appl. Polym. Sci., **101**(6), pp. 3806–3810.
[46] Feng, M., Pan, Y., Zhang, M., Gao, Q., Liu, C., Shen, C., and Liu, X., 2021, "Largely Improved Thermal Conductivity of Hdpe Composites by Building a 3D Hybrid Fillers Network," Compos. Sci. Technol., **206**, p. 108666.
[47] Weidenfeller, B., Höfer, M., and Schilling, F. R., 2004, "Thermal Conductivity, Thermal Diffusivity, and Specific Heat Capacity of Particle Filled Polypropylene," Compos. A: Appl. Sci. Manuf., **35**(4), pp. 423–429.
[48] Chen, L., Xu, H.-F., He, S.-J., Du, Y.-H., Yu, N.-J., Du, X.-Z., Lin, J., and Nazarenko, S., 2017, "Thermal Conductivity Performance of Polypropylene Composites Filled With Polydopamine-Functionalized Hexagonal Boron Nitride," PLOS One, **12**(1), p. e0170523.
[49] Kalakonda, P., Cabrera, Y., Judith, R., Georgiev, G. Y., Cebe, P., and Iannacchione, G. S., 2015, "Studies of Electrical and Thermal Conductivities of Sheared Multi-Walled Carbon Nanotube With Isotactic Polypropylene Polymer Composites," Nanomater. Nanotechnol., **5**, p. 2.
[50] Lua, A. C., and Su, J., 2006, "Isothermal and Non-Isothermal Pyrolysis Kinetics of Kapton Poyimide," Polym. Degrad. Stab., **91**(1), pp. 144–153.
[51] Montgomery, D. C., and Runger, G. C., 2010, *Applied Statistics and Probability for Engineers*, John Wiley & Sons, Hoboken, NJ.
[52] Zheng, Q., Kaur, S., Dames, C., and Prasher, R. S., 2020, "Analysis and Improvement of the Hot Disk Transient Plane Source Method for Low Thermal Conductivity Materials," Int. J. Heat Mass Transf., **151**, p. 119331.
[53] Zhang, H., Li, M., Fang, W., Dan, D., Li, Z., and Tao, W., 2014, "A Numerical Study on the Theoretical Accuracy of Film Thermal Conductivity Using Transient Plane Source Method," Appl. Therm. Eng., **72**(1), pp. 62–69.
[54] Wei, Q., Uehara, C., Mukaida, M., Kirihara, K., and Ishida, T., 2016, "Measurement of in-plane Thermal Conductivity in Polymer Films," AIP Adv., **6**(4), p. 045315.
[55] Kommandur, S., and Yee, S., 2018, "A Suspended 3-Omega Technique to Measure the Anisotropic Thermal Conductivity of Semiconducting Polymers," Rev. Sci. Instrum., **89**(11).
[56] Bounioux, C., Díaz-Chao, P., Campoy-Quiles, M., Martín-González, M. S., Goni, A. R., Yerushalmi-Rozen, R., and Müller, C., 2013, "Thermoelectric Composites of Poly (3-hexylthiophene) and Carbon Nanotubes With a Large Power Factor," Energy Environ. Sci., **6**(3), pp. 918–925.
[57] Kiefer, D., Yu, L., Fransson, E., Gómez, A., Primetzhofer, D., Amassian, A., Campoy-Quiles, M., and Müller, C., 2017, "A Solution-Doped Polymer Semiconductor: Insulator Blend for Thermoelectrics," Adv. Sci., **4**(1), p. 1600203.